Rational Design of Mesoporous Carbon Electrodes with High Mass Loading for Binder-Free Supercapacitors

Xiang-Qian Zhang, Wei Dong, An-Hui Lu, and Wen-Cui Li*[a]

A three-dimensional mesoporous carbon/nickel foam hybrid material has been prepared using an in situ solution growth approach, and its energy storage as a binder-free supercapacitor electrode is explored. The nickel foam is chosen as an electrically conducting scaffold and also as a porous substrate for the growth of poly(benzoxazine-co-resol). After carbonization, tightly packed carbon layers are uniformly coated on the skeleton of the nickel foam. Such carbons show hierarchical porosity (micro-, meso-, macroporosity), a high surface area of $811\ m^2g^{-1}$, and graphitic domains. These features allow easy access, rapid diffusion, and a high loading of ions, producing a material in which ion diffusion is faster than in bulk carbon and which is highly efficient in producing an increased double-layer capacitance. The obtained electrodes exhibit an excellent capacitive behavior in KOH solutions, that is, low contact resistance, high specific capacitance ($192\ Fg^{-1}$), and good rate performance. Furthermore, the three-dimensional porous substrates facilitate a high mass loading of active materials, up to $21\ mg\,cm^{-2}$, and per-area capacitance of $1.18\ F\,cm^{-2}$. This synthesis strategy is scalable and potentially usable for large-scale production.

Introduction

With the rapid growth of the global population and economy, there is increasing demand for clean energy. Supercapacitors are considered to be the most promising energy storage and power output technologies due to their high power density, long cycling stability, and low environmental impact.[1–7]

During recent years, enormous effort has been dedicated to the development of novel micro-/nano-structured electrode materials for fabricating ideal energy storage devices.[8–15] Such structures, consisting of binder-free networks, provide pathways for both electrons and ions in the electrodes. Recently, researchers have shown great interest in developing novel fabrication strategies by using mild synthesis conditions for binder-free energy devices, which have significant advantages over traditional methods, such as producing a high effective surface area, high conductivity, and being easy to synthesize.[16–20] In this regard, several strategies such as electroplating,[20,21] chemical vapor deposition,[22] and layer-by-layer deposition processes[23] have been developed to prepare binder-free electrodes, where the active materials directly "grow" on the metal substrate. Using these methods, one can improve the internal binding between the active materials and metal current collectors, and thus produce electrodes with very small resistances. Various kinds of active materials including Ni/MnO_2,[20] vertically aligned carbon nanotube (CNT) arrays,[21] TiO_2/anatase/carbon,[23] MnO_x/CNT,[24] graphene hydrogels,[25,26] and nanosheets[27–29] have been deposited on the nickel foam or other current collectors for binder-free energy storage devices. Among various supercapacitor substrates, nickel foams are recognized to show many advantages because their 3D structure provides both excellent contact between the electrodes and aqueous electrolytes, and also diffusion channels for electrolyte ions, thus improving the energy storage performance.[30–33]

Mesoporous carbon is one of the most promising materials for electric double-layer capacitors (EDLCs) given its low-cost, high specific surface area, and easily accessible mesopore channels.[22,34–37] Because the regular network of interconnected pore channels in the mesopore range facilitates ion transport and shortens diffusion pathways, mesoporous carbon has a far better rate capability than other carbon-based materials.[9,38,39] However, the majority of approaches to prepare carbon electrodes involve the use of binders and conductive additives. This considerably increases the contact resistance and is undesirable for the efficient charge and mass exchange that occurs upon charging/discharging. Besides, the fabrication of these electrode structures usually requires complex procedures depending on the specific electrochemically active material that is used. The per-area mass loading of active material through the whole electrodes is always limited. Therefore, it is highly desirable, but challenging, to develop a simple and efficient route for synthesis of binder-free porous carbon electrodes.

Here, we report a novel approach to the direct fabrication of mesoporous carbon (MC) electrodes by in situ growth and subsequent carbonization, without using any binder, conduc-

[a] X.-Q. Zhang, W. Dong, Prof. Dr. A.-H. Lu, Prof. Dr. W.-C. Li
State Key Laboratory of Fine Chemicals, School of Chemical Engineering
Dalian University of Technology
Dalian 116024 (PR China)
Fax: (+ 86)-411-84986355
E-mail: wencuili@dlut.edu.cn

These are not the final page numbers! ↗↗

tive additives, or slurry-coating procedures. The strategy is based on fast self-assembly and polymerization that directly uses benzoxazine oligomers as building blocks. During subsequent heat treatment, tightly packed carbon layers with high surface area and accessible mesopore channels are formed from decomposition of the carbon precursors [i.e., poly(benzoxazine-co-resol)]. The mass loading of mesoporous carbon coatings can be controlled by tuning the concentration of carbon precursor and the deposition time. The synthesis is easy and potentially usable for large-scale production. The developed mesoporous carbon electrodes with a high mass loading (≈ 10 mg cm^{-2}), hierarchical porosity, and high conductivity show excellent capacitive behavior in a KOH electrolyte, that is, a specific capacitance of 192 F g^{-1} at a current density of 0.5 A g^{-1}. Efforts have also been made to achieve synergistic integration of graphene and mesoporous carbon, where an electrode based on a graphene-containing mesoporous carbon is prepared by a similar method, demonstrating the versatility of this approach for preparing carbon-metal hybrid materials. Such a simple and versatile fabrication method shows great promise in the preparation of various binder-free hybrid electrodes.

Results and Discussion

The overall synthesis procedure leading to 3D mesoporous carbon/nickel foam structures is illustrated in Scheme 1. The nickel foam (NF), a porous structure with an interconnected 3D scaffold of nickel, was chosen as a template for the in situ growth of porous carbon coatings on the nickel foam through an aqueous deposition and subsequent carbonization process (Scheme 1). First, the 3D nickel foam was dipped into the precursor solution. To minimize electrolyte ion diffusion limitation, surfactant Pluronic F127 was used in the reaction system to direct the formation of mesopores during the assembly of poly(benzoxazine-co-resol). In this step, the precursor solution was expected to

be uniformly adsorbed and deposited on the surface of the nickel foam, due to the good wettability and rapid assembly of the carbon precursor, driven by the strong interfacial interaction between the amine-participating sol-gel system and the nickel foam grid structure.[23] After heat treatment at 90 °C and subsequent carbonization at 800 °C in an Ar atmosphere, the mesoporous carbon-coated 3D nickel foam (NF@MC-1) was obtained. Then, the newly developed NF@MC hybrids were directly used as binder-free electrodes in supercapacitors. Compared to the majority of traditional electrodes, this novel in situ growth strategy avoids complicated procedures and is potentially scalable for fabricating binder-free supercapacitor.

The structure of the NF@MC-1 was investigated by using scanning electron microscopy (SEM), as shown in Figure 1. SEM images with different resolutions clearly showed that the porous carbon has been continuously coated onto the surface of the nickel foam skeleton (Figure 1a and b) and the carbon coatings show a tightly packed layer structure (Figure 1c and d). Representative optical photographs (Supporting Information, Figure S1) show that the nickel foam changes color from silvery luster, yellow to black, clearly indicating the homogeneous deposition of the precursor solution, polymer, and carbon. Further, as seen in Figure 1a and b, there are no bulk carbon particles for NF@MC-1, suggesting that carbon layers are uniformly coated on the nickel foam. Macropores with sizes from 100 to 500 μm are also
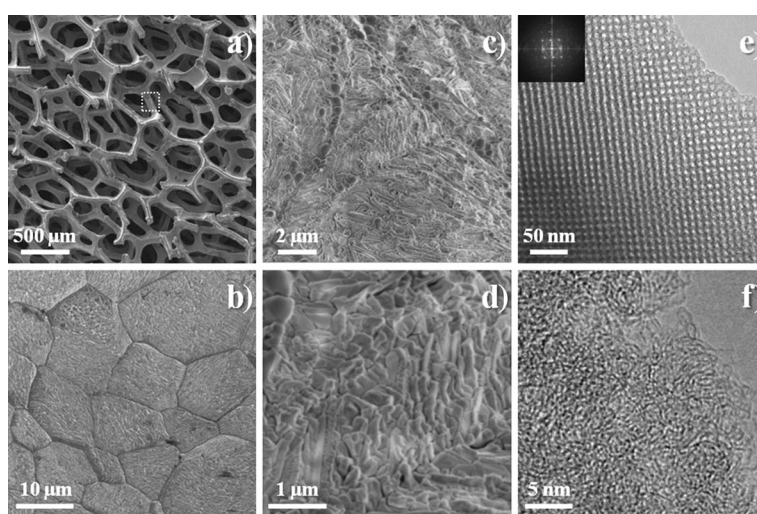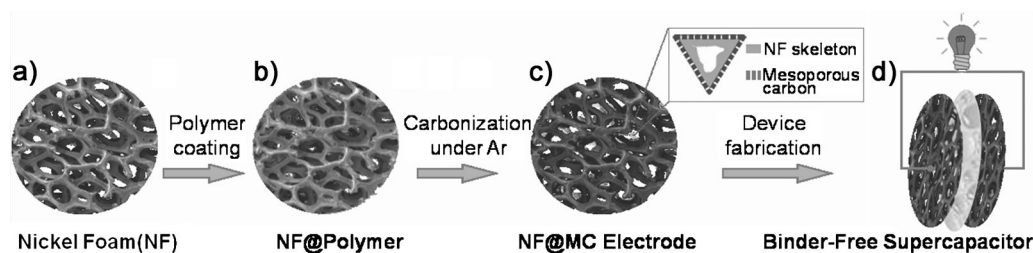

Figure 1. a–d) SEM images of NF@MC-1 electrodes and e,f) TEM images of MC-1.


Scheme 1. Schematic for the in situ growth of the mesoporous carbon on nickel foam.

preserved, without collapsing and cracking, indicating that the introduction of the porous carbon matrix does not damage the scaffold. As shown in Figure S2 (Supporting Information), the red spot lines were marked to indicate the thickness and morphology of the loaded carbon. Interestingly, by utilizing the entire 3D nickel foam structure, the carbon thickness of our developed electrode with high mass loading of 10 mg cm^{-2} is only approximately 1–5 μm (Supporting Information, Figure S2), much thinner than that of traditional electrodes ($\geq$100 μm) under the same areal mass loading of active materials. Thus, the electrolyte solution can easily penetrate the large voids in the nickel foam and contribute to the double-layer capacitance on the carbon surface throughout the entire network. For comparison, mesoporous carbon (MC-p) and the microporous carbon/NF hybrid (NF@MC-2) were also synthesized using the same method but without use of nickel foam and F127, respectively. SEM images (Supporting Information, Figure S3) of MC-p show large spherical grains on the micrometer scale (even tens of micrometers) indicating the shape- and structure-directing effect of the nickel foam during the formation of the carbon coatings with a tightly packed structure.

Furthermore, the transmission electron microscope (TEM) images (Figure 1 e and Figure S4, Supporting Information) clearly prove the regular mesopores of MC-1 and the pore size is estimated to be 5–7 nm. The fast Fourier transform (FFT) diffractograms also clearly confirm the presence of an interconnected cubic (Im3m) mesopore system.[40,47] Thus, ion/electron transport distances in the electrodes were shortened as a result of the unique open pore system and unique structure of such a carbon electrode. Notably, the high resolution TEM image of MC-1 (Figure 1 f) shows a partially graphite-like microstructure, which may be due to the catalytic graphitization effect of metallic nickel. Compared to a completely amorphous carbon, local graphitic domains can endow the as-prepared porous carbon with good electrical conductivity.[8] Such highly conductive electrodes with optimized structures for easy ion/electron transport are indispensable for fabricating ideal EDLCs.

To further investigate the detailed textural characteristics of the obtained carbons, N$_2$ adsorption–desorption measurements were performed (Figure 2 a). The adsorption–desorption isotherms of MC-1 and MC-p exhibit the prominent characteristics of type-IV isotherms with a distinct hysteresis loop in the P/P_0 range of 0.4–0.8, implying the presence of relatively large mesopores. The adsorption isotherm of MC-2 is of type I, reflecting its microporosity. Moreover, as shown in Figure 2 b, the pore sizes of both MC-1 and MC-p calculated by the Barrett–Joyner–Halenda (BJH) method are concentrated at 5.2 nm, indicating a mesoporous structure. The TEM image in Figure 1 e also indicates the presence of such mesopores, which can be attributed to the decomposition of surfactant F127 during pyrolysis. Brunauer–Emmett–Teller (BET) analysis reveals a specific surface area of 811 m^2 g^{-1} for MC-1, slightly higher than that (734 m^2 g^{-1}) of MC-p, and much higher than that (533 m^2 g^{-1}) of MC-2 (Table 1). This is ascribed to the unique thin layer structure of MC-1 giving it
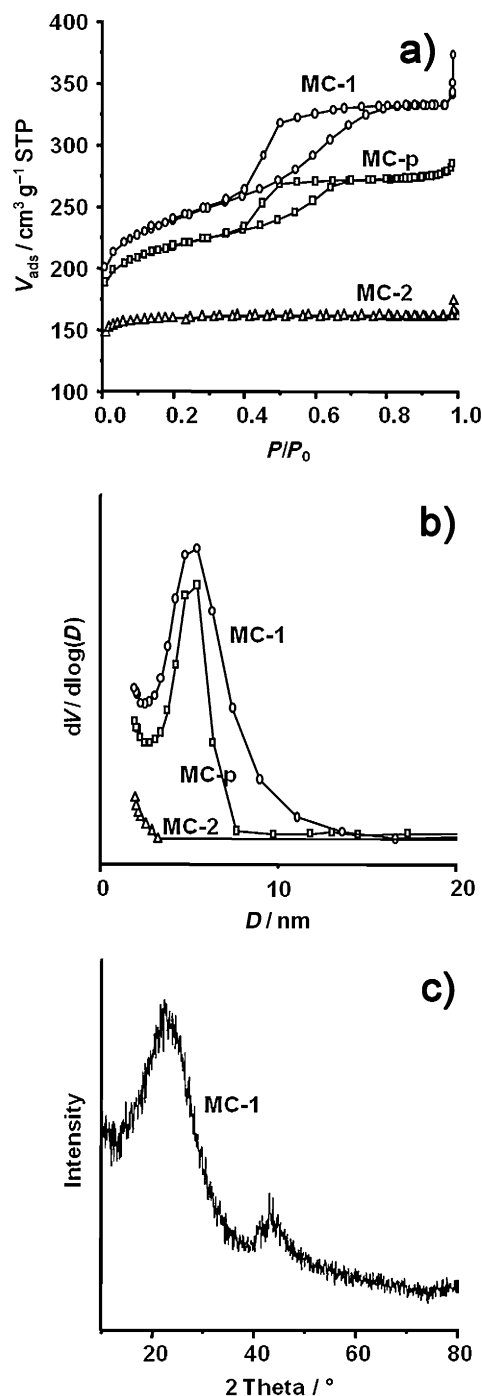
Figure 2. a) Typical N$_2$ adsorption-desorption isotherms and b) Pore size distributions (PSDs) of the three carbon samples MC-1, MC-2, and MC-p; c) XRD pattern of MC-1.

more S_{BET} than MC-p (which is composed of large micrometer-sized spherical grains) and microporous MC-2. X-ray diffraction (XRD) of MC-1 exhibits a strong peak at 25° (2θ) and a weaker peak at 43.2°, which are attributed to the (002) and (100) planes, respectively. Such suitably developed interconnected meso-/micropores are of great importance to the electrochemical performance.

The aforementioned characterization results confirm that the current synthesis is simple and effective in producing

© 2015 Wiley-VCH Verlag GmbH & Co. KGaA, Weinheim

These are not the final page numbers! ↗↗

Table 1. Structural parameters of the porous carbon samples.

| Sample	S_{BET} [m^{2}g^{-1}]	S_{micro} [m^{2}g^{-1}]	D_{peak} [nm]	V_{total} [cm^{3}g^{-1}]	V_{micro} [cm^{3}g^{-1}]
MC-1	811	579	5.2	0.576	0.268
MC-2	533	494	-	0.267	0.229
MC-p	734	577	5.2	0.439	0.267

mesoporous carbon electrodes. More importantly, such hybrid materials can be directly used as binder-free supercapacitor electrodes without adding any binder or conductive additives. Considering these attractive features, the electrochemical performances of NF@MC-1, NF@MC-2, and NF/MC-p electrodes were evaluated in a 6 M KOH aqueous electrolyte. First, the correlation between the microstructure and capacitance of samples is discussed. Because of the large specific surface area, unique mesoporosity, and shortened diffusion paths, the NF@MC-1 electrode is expected to be an excellent candidate for high-performance supercapacitors. The electrochemical results for these carbon electrodes are shown in Figure 3. The cyclic voltammetry (CV) curves of the three samples show a typical quasi-rectangular shape at a scan rate of 10 mV s^{-1}, characteristic of a double layer capacitor, indicating good charge propagation at the electrode interfaces following the EDLC mechanism. Herein, it should be noted that the capacitance contribution from the nickel foam can be neglected (see Figure S5, Supporting Information). The obtained NF@MC-1 shows a specific capacitance as high as 180 F g^{-1} at a scan rate of 5 mV s^{-1}, a value nearly twice that of the MC-p electrode fabricated through the traditional slurry-coating process (Figure 3c), which clearly

demonstrates the superiority of our newly developed in situ growth method. As shown in Figure 3b, the galvanostatic charge–discharge curves have a symmetric triangular shape, which also reflects a typical electric double layer capacitance. As expected, the highest specific capacitance is observed for NF@MC-1 electrodes and can reach a value as high as 192 F g^{-1}, which is higher than that of NF@MC-2 (174 F g^{-1}) and NF/MC-p (126 F g^{-1}). As a result, the specific capacitance of such a NF@MC-1 is comparable to, or even higher than those of porous carbon-based electrodes reported recently,[41–44] as shown in Table S1 (Supporting Information).

To verify the versatility of this in situ growth approach, we also introduced graphene into the precursor for the carbon–metal hybrid electrodes. As shown in Figure S6 (Supporting Information), a graphene-containing porous carbon/NF hybrid (NF@MC-1-G) was also prepared and its pore structure and morphology were measured, showing similarity with NF@MC-1. The S_{BET} of NF@MC-1-G is 758 m^{2}g^{-1} and the pore size of MC-1-G (calculated by using the BJH method) is concentrated at 5.2 nm (Figure S6d, Supporting Information). Further, the capacitive performance of NF@MC-1-G-based devices were also measured (Supporting Information, Figure S7). NF@MC-1-G showed slightly lower performance at lower rates in comparison to NF@MC-1, possibly due to its lower surface area than that of NF@MC-1 (811 m^{2}g^{-1}). However, NF@MC-1-G exhibited a somewhat better rate capability than NF@MC-1 due to the synergistic effect of the integration of graphene and mesoporous carbon. These parallel experiments strongly suggest the critical importance of integrating a highly interconnected scaffold, unique hierarchical porosity, and low contact resistance to improve the electrochemical performance of the mesoporous carbon samples. These features allow easy access, rapid diffusion, and a high loading of ions; as a result the material outperforms the ion diffusion rate in bulk carbon electrodes and produces an increased double-layer capacitance.

Electrochemical impedance spectroscopy (EIS) was used to determine the ion transport behavior and electrical resistance of the NF@MC-1, NF@MC-2, NF/MC-p, and NF@MC-1-G electrodes. Figure 4a shows Nyquist plots based on a frequency response analysis of frequencies ranging from 1 MHz to 10 mHz. The impedance curve intersects the real
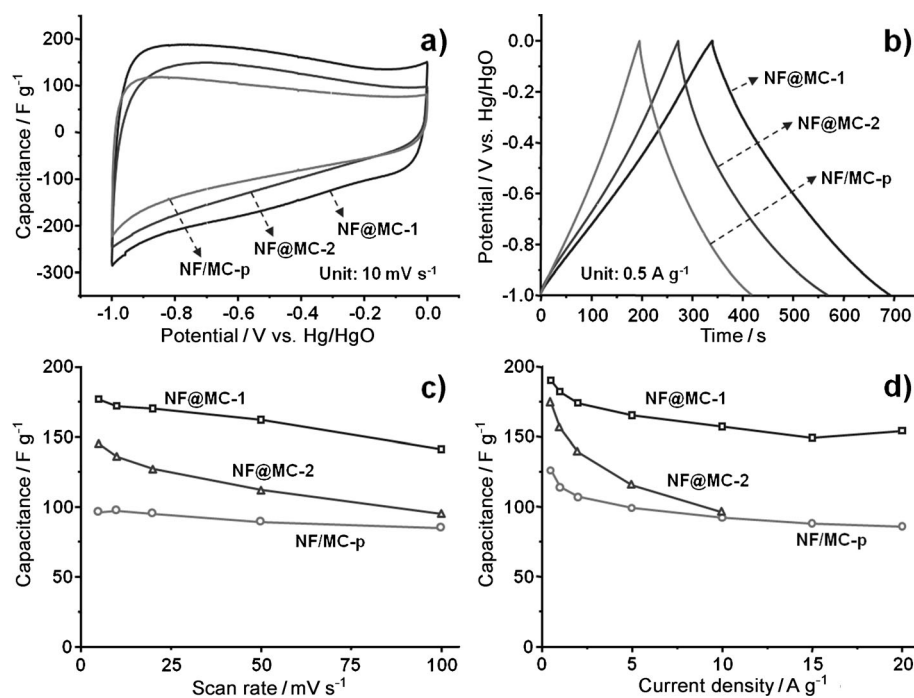
Figure 3. Electrochemical performance of the obtained carbon electrodes: a) CV curves tested at a scan rate of 10 mV s^{-1}; b) Galvanostatic charge–discharge curves tested at a current density of 0.5 A g^{-1}; c) Capacity profiles at different scan rates; and d) different applied current densities.

These are not the final page numbers! ↗↗
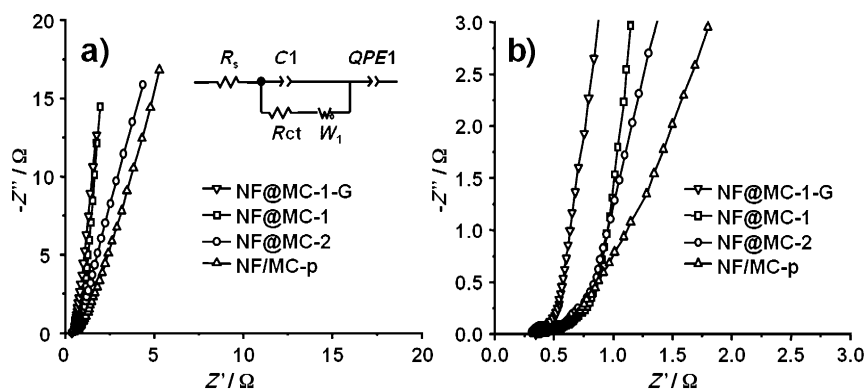
Figure 4. a) Electrochemical impedance spectra under the influence of an AC voltage (5 mV). Inset: Equivalent circuit for the simulation of the impedance spectra of the capacitor cells; b) Magnification of the high-frequency region.

axis at a 45° angle at the beginning, which is typical of a porous electrode that is saturated with electrolyte. At low frequencies, the straight line tends to be perpendicular to the real axis, indicating the pure capacitive behavior of NF@MC-1 and NF@MC-1-G. The inset of Figure 4a shows an equivalent circuit model to simulate the capacitive and resistive elements of the cells under analysis. The elements include the internal resistance (R_s), the charge transfer resistance (R_{ct}), a Warburg diffusion element attributed to ion migration through the carbon coatings (Z_w), and the capacitance (QPE). By fitting the impedance data to this model, fitting parameters were thus obtained (Table 2). As shown, the equivalent series resistances (ESR) of NF@MC-1, NF@MC-1-G, NF@MC-2, and NF/MC-p are calculated to be 0.401, 0.345, 0.383, and 0.428 Ω, respectively. As expected, the relatively small ESR values of NF@MC-1 and NF@MC-1-G are observed due to the existence of a 3D network structure that can facilitate the efficient access of electrolyte ions to the carbon surface and shorten the ion diffusion path. As shown in Figure 4b, lines at low frequency are observed for NF@MC-1 and NF@MC-1, indicating good electrical conductivity and fast ion diffusion behavior due to the well-defined mesoporosity, high surface area, and thin layered carbon coating, which together allow a high loading of charged ions and an easy access for the electrolyte ions.

The electrochemical performance of the NF@MC-1 based supercapacitor was also measured in a two-electrode test system (Figure 5). The capacitive performance of the carbon-based electrodes was evaluated by CV and galvanostatic charge–discharge measurement. The CV curve of NF@MC-1 at the scan rate of 200 mV s⁻¹ showed a relatively good rectangular profile indicating the typical characteristics of double-layer capacitance. Further, as can be seen in Figure 5b, galvanostatic charge–discharge experiments were performed and all charge/discharge curves retained isosceles triangle shapes at current densities ranging from 0.5 to 5 A g⁻¹, and only a slight change in the specific capacitance was observed. The NF@MC-1 electrode has a high specific capacitance of 136 F g⁻¹ at 0.5 A g⁻¹, and retains a capacitance of 87 F g⁻¹ at 5 A g⁻¹, indicating good rate capability. The NF@MC-1 elec-

Table 2. EIS analysis of the prepared samples.

Sample	R_s [Ω]	R_{ct} [Ω]	Z_w [Ω s⁻¹]	$QPE1$
NF@MC-1	0.401	0.100	0.285	1.338
NF@MC-1-G	0.345	0.017	0.063	1.345
NF@MC-2	0.383	0.197	0.311	1.141
NF/MC-p	0.428	0.108	0.649	0.312
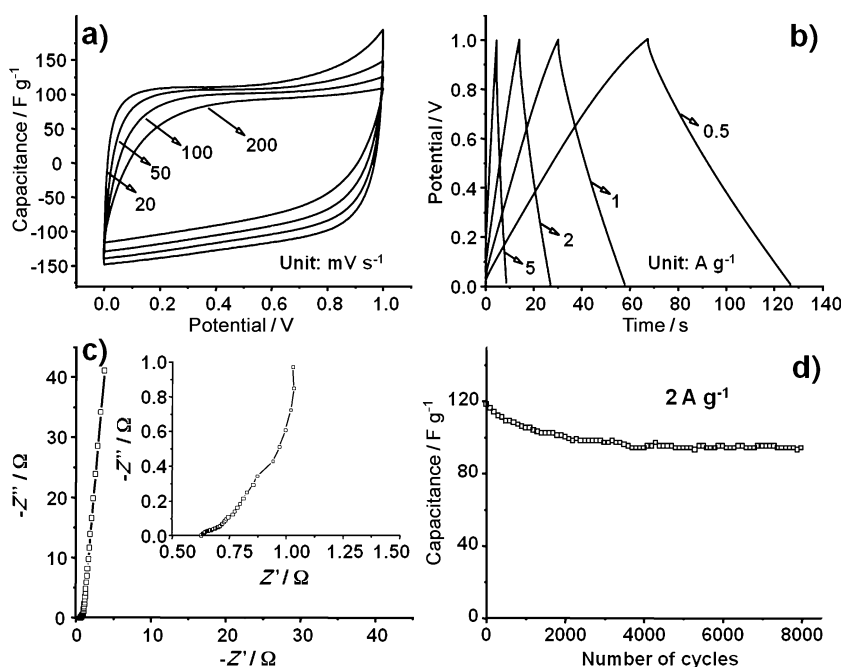
Figure 5. Electrochemical performance of NF@MC-1 with a mass loading of 10 mg cm⁻² tested in a two-electrode system: a) CV curves at various scan rates; b) Galvanostatic charge–discharge curves under different current densities; c) Capacity profiles at different current densities; d) The long cycle life over 8000 cycles tested at a current density of 2 A g⁻¹.

trode also has an excellent cycling stability, retaining approximately 80% of its initial capacitance after 3000 charging/discharging cycles and remaining unchanged till 8000 cycles (Figure 5). Upon comparing our results with those from the literature, it is clear that the capacitance value of NF@MC-1 is close to or better than that of other porous carbon electrodes (Table S1, Supporting Information). In addition, the overall size, shape, and mass loading of the obtained electrode can be easily controlled by using varied nickel foam substrates, precursor solutions, deposition times, etc. As a proof-of-concept experiment, the mass loading of NF@MC-1 was increased to 21 $mg\,cm^{-2}$ and the electrochemical performance is shown in Figure S8 (Supporting Information). It can be seen that the CV curves remained quasi-rectangular and the per-area capacitance reached 1.18 $F\,cm^{-2}$, which is comparable to or even better than previously reported values.[45,46]

The synergistic effect of the multicomponent structures has been validated: i) conductive foams with 3D frameworks offer multidimensional pathways to facilitate the transport of electrons within the bulk electrode; ii) well-defined mesoporous channels are favorable for buffering ions to shorten the diffusion distances from the external electrolyte to the interior surfaces; iii) in situ formed tightly packed carbon layers can further increase ion transport and charge storage capacity. Further, the synthesis is simple and potentially scalable for production because it is binder-free and avoids using conductive additives and grinding procedures.

Conclusions

We have demonstrated a new mesoporous carbon/nickel foam hybrid material using a simple and mild in situ growth approach and explored its energy storage application as a binder-free supercapacitor electrode. By simple solution polymerization and subsequent carbonization, mesoporous carbon with high mass loading, high surface area, and hierarchical porosity can be deposited on a 3D nickel foam framework. The obtained carbon/nickel foam hybrids can be directly used as binder-free electrodes. Such an approach avoids the use of binder, conductive additives, and slurry-coating procedures, which facilitates fast transfer of electrons and ions in the electrodes. Thus, the newly developed mesoporous carbon electrode with high mass loading exhibits satisfactory double-layer capacitive behavior with high rate capability and high specific capacitance (192 $F\,g^{-1}$). This study may provide a new procedure to construct binder-free supercapacitors and extend the potential application of porous carbon-based devices.

Experimental Section

Chemicals

Resorcinol (R, 99.5%) was purchased from Tianjin Kermel Chemical Reagent Co., Ltd. Formaldehyde solution (F, 37 wt%), 1,6-diaminohexane (DAH, 99.0%), and ethanol (99.7%) were

supplied by Sinopharm Chemical Reagent Co., Ltd. Triblock copolymer Pluronic F127 ($M_w = 12\,600$, $PEO_{106}PPO_{70}PEO_{106}$) was purchased from Sigma–Aldrich. All chemicals were used as received. Graphene oxide (GO) colloids were prepared following a modified Hummers method.[10] The nickel foams (NF, Changsha Lyrun New Material Co. Ltd., China) with a size of 0.1 cm in thickness and approximately 40 $mg\,cm^{-2}$ in areal density were washed in deionized water and acetone before use.

Synthesis of mesoporous carbon electrodes

Resorcinol and Pluronic F127 with a molar ratio of 275:1 were dissolved in a 4.5 g solvent mixture of ethanol and deionized water (mass ratio of 1:1) with magnetic stirring at 25°C. Afterwards, 1,6-diaminohexane (0.019 g) was added to the above solution and stirred for 10 min at 25°C. A certain amount of formalin (37 wt%) was then quickly injected into the solution. The reaction system instantaneously (<1 min) turned to a white homogeneous emulsion, and the reaction mixture was stirred at 25°C for another 10 min. A circular piece of nickel foam with diameter of 1.6 cm was immersed in the emulsion under ultrasound for 5 min to ensure the adsorption and self-assembly of the carbon precursor on the nickel foam. The obtained hybrid material was then pulled out and dried at 90°C for 4 h followed by pyrolysis at 800°C for 2 h under an Ar atmosphere to obtain mesoporous carbon electrodes (NF@MC-1). Then the samples were put into a HCl (6 M) solution at 80°C for 3 h to completely dissolve the nickel and obtain MC-1. Sample (MC-p) was fabricated according to our previously reported work,[47] which is identical to that of NF@MC-1 but without the use of nickel foam. For comparison, two other porous carbon electrodes were prepared. These are (a) a microporous carbon electrode (NF@MC-2) prepared using the same synthesis procedure except for the absence of F127 and (b) a sample (NF@MC-1-G) with added graphene obtained by adding an addition of graphene oxide (1.0 mg) to the homogeneous emulsion of NF@MC-1 while retaining the other conditions. In all the syntheses, the molar ratio between resorcinol and formaldehyde was maintained at 1:2.

Characterization

Transmission electron microscope (TEM) images of the samples were obtained using a Tecnai $G^2$20S-Twin electron microscope equipped with a cold field emission gun. The acceleration voltage was 200 kV. Samples were prepared by adding a few drops of a suspension of one sample in ethanol onto a holey carbon grid with a pipette. Scanning electron microscope (SEM) investigations were performed using a NOVA NanoSEM 450 instrument, operated at 3 kV or 10 kV. The nitrogen sorption measurements were performed using a Tristar 3000 adsorption analyzer (Micromeritics). The Brunauer–Emmett–Teller (BET) method was used to calculate the specific surface areas (S_{BET}) using adsorption data in the relative pressure interval of 0.06–0.2. Pore size distribution (PSD) curves were calculated by using the BJH (Barrett–Joyner–Halenda) method from the adsorption branch. The total pore volume (V_{total}) was estimated from the amount adsorbed at a relative pressure of 0.99. Micropore surface area (S_{micro}) and micropore volumes (V_{micro}) were calculated using the t-plot method, and single-point pore volume (V_{total}) from adsorption isotherms at $P/P_0 = 0.99$. The mesopore volume (V_{meso}) was obtained by deducting the micropore volume from the total volume. X-ray diffraction (XRD) patterns of samples were recorded using a Rigaku D/Max 2400 diffractometer in the Bragg

These are not the final page numbers! ↗↗

Brentano (reflection) geometry and Cu$_{K\alpha}$ radiation ($\lambda = 0.15406$ nm).

Electrochemical Evaluation

The NF@MC-1, NF@MC-2, and NF@MC-1-G were directly used as the working electrodes. As a contrast, the working electrode NF/MC-p was fabricated by physically mixing 80 wt% carbon materials (MC-p), 10 wt% polytetrafluoroethylene (PTFE), and 10 wt% conductive carbon black, and then pressing onto a nickel foam to serve as a current collector. The mean mass loading of the carbon of all the electrodes was approximately 10 mg cm^{-2}. The electrochemical measurements were performed using a conventional three-electrode system with the obtained electrodes serving as the working electrode, a platinum plate as counter electrode, a Hg/HgO electrode (0.052 V vs. a normal hydrogen electrode, NHE) as reference electrode, and 6 M KOH as an aqueous electrolyte. The electrochemical performance of a single electrode was tested on a CHI660D electrochemical workstation (CH Instruments Inc., Shanghai, China). Cyclic voltammetry (CV), electrochemical impedance spectroscopy (EIS), and galvanostatic charge–discharge tests were used in the evaluation of the electrode electrochemical performance in a three-electrode system at room temperature. The specific gravimetric capacitance of the single electrode derived from the CV tests was calculated using Equation (1):[48]

$$C_s(F/g) = \frac{i}{mv} \qquad (1)$$

in which m (g), i (A), and v (V s^{-1}) are the mass of the active electrode material, the current (its value at -0.5 V is used here for calculations), and the scan rate, respectively. EIS measurements were performed at an alternating current (AC) amplitude of 5 mV in the range of from 100 kHz to 10 mHz. Symmetrical supercapacitors were fabricated using two identical NF@MC-1 electrodes and a filter paper separator (MPF50AC purchased from Nippon Kodoshi plant, Japan) immersed in a 6 M KOH aqueous electrolyte solution. The long cycle life was measured using an Arbin SCTS-165699-T multichannel electrochemical workstation.

Acknowledgements

Keywords: binder-free electrodes · carbonization · mesoporous carbon · nickel · supercapacitors

[1] X. Lu, M. Yu, G. Wang, Y. Tong, Y. Li, *Energy Environ. Sci.* **2014**, *7*, 2160.

[2] J. Yan, Q. Wang, T. Wei, Z. Fan, *Adv. Energy Mater.* **2014**, *4*, 1300816.

[3] P. Simon, Y. Gogotsi, *Acc. Chem. Res.* **2013**, *46*, 1094.

[4] Y.-G. Wang, H. Q. Li, Y.-Y. Xia, *Adv. Mater.* **2006**, *18*, 2619.

[5] Y. Zhu, S. Murali, M. D. Stoller, K. J. Ganesh, W. Cai, P. J. Ferreira, A. Pirkle, R. M. Wallace, K. A. Cychosz, M. Thommes, D. Su, E. A. Stach, R. S. Ruoff, *Science* **2011**, *332*, 1537.

[6] H. Chen, W. Dong, J. Ge, C. Wang, X. Wu, W. Lu, L. Chen, *Sci. Rep.* **2013**, *3*, 1910.

[7] A. Burke, *Electrochim. Acta* **2007**, *53*, 1083.

[8] D.-C. Guo, J. Mi, G.-P. Hao, W. Dong, G. Xiong, W.-C. Li, A.-H. Lu, *Energy Environ. Sci.* **2013**, *6*, 652.

[9] Y. Korenblit, M. Rose, E. Kockrick, L. Borchardt, A. Kvit, S. Kaskel, G. Yushin, *ACS Nano* **2010**, *4*, 1337.

[10] J. Zhang, Y.-X. Yin, Y. You, Y. Yan, Y.-G. Guo, *Energy Technol.* **2014**, *2*, 757.

[11] G.-P. Hao, A.-H. Lu, W. Dong, Z.-Y. Jin, X.-Q. Zhang, J.-T. Zhang, W.-C. Li, *Adv. Energy Mater.* **2013**, *3*, 1421.

[12] P. Simon, Y. Gogotsi, *Nat. Mater.* **2008**, *7*, 845.

[13] M. Antonietti, N. Fechler, T.-P. Fellinger, *Chem. Mater.* **2014**, *26*, 196.

[14] Z. Chen, Y. Yuan, H. Zhou, X. Wang, Z. Gan, F. Wang, Y. Lu, *Adv. Mater.* **2014**, *26*, 339.

[15] O. Rios, S. K. Martha, M. A. McGuire, W. Tenhaeff, K. More, C. Daniel, J. Nanda, *Energy Technol.* **2014**, *2*, 773.

[16] J. W. Long, B. Dunn, D. R. Rolison, H. S. White, *Chem. Rev.* **2004**, *104*, 4463.

[17] D. R. Rolison, J. W. Long, J. C. Lytle, A. E. Fischer, C. P. Rhodes, T. M. McEvoy, M. E. Bourg, A. M. Lubers, *Chem. Soc. Rev.* **2009**, *38*, 226.

[18] H. Ji, L. Zhang, M. T. Pettes, H. Li, S. Chen, L. Shi, R. Piner, R. S. Ruoff, *Nano Lett.* **2012**, *12*, 2446.

[19] S. Li, D. Huang, B. Zhang, X. Xu, M. Wang, G. Yang, Y. Shen, *Adv. Energy Mater.* **2014**, *4*, 1301655.

[20] Z. Su, C. Yang, B. Xie, Z. Lin, Z. Zhang, J. Liu, B. Li, F. Kang, C. P. Wong, *Energy Environ. Sci.* **2014**, *7*, 2652.

[21] Y. Jiang, P. Wang, J. Zhang, W. Li, L. Lin, *Proc. IEEE MEMS* (Hong Kong), Jan. **2010**.

[22] J. Zhi, W. Zhao, X. Liu, A. Chen, Z. Liu, F. Huang, *Adv. Funct. Mater.* **2014**, *24*, 2013.

[23] X. Wang, Y. Yan, B. Hao, G. Chen, *ACS Appl. Mater. Interfaces* **2013**, *5*, 3631.

[24] J. Li, Q. M. Yang, I. Zhitomirsky, *J. Power Sources* **2008**, *185*, 1569.

[25] J. Chen, K. Sheng, P. Luo, C. Li, G. Shi, *Adv. Mater.* **2012**, *24*, 4569.

[26] S. Ye, J. Feng, P. Wu, *ACS Appl. Mater. Interfaces* **2013**, *5*, 7122.

[27] Y. Chen, X. Zhang, P. Yu, Y. Ma, *J. Power Sources* **2010**, *195*, 3031.

[28] Z. Chen, W. Ren, L. Gao, B. Liu, S. Pei, H.-M. Cheng, *Nature* **2011**, *10*, 424.

[29] J. Chen, K. Sheng, P. Luo, C. Li, G. Shi, *Adv. Mater.* **2012**, *24*, 4569.

[30] J. Jiang, Y. Y. Li, J. P. Liu, X. T. Huang, C. Z. Yuan, X. W. Lou, *Adv. Mater.* **2012**, *24*, 5166.

[31] J. Pu, Y. Tong, S. Wang, E. Sheng, Z. Wang, *J. Power Sources* **2014**, *250*, 250.

[32] X. Cao, Y. Shi, W. Shi, G. Lu, X. Huang, Q. Yan, Q. Zhang, H. Zhang, *Small* **2011**, *7*, 3163.

[33] C. Z. Yuan, L. Yang, L. R. Hou, L. F. Shen, X. G. Zhang, X. W. Lou, *Energy Environ. Sci.* **2012**, *5*, 7883.

[34] J. Liu, T. Yang, D.-W. Wang, G. Q. Lu, D. Zhao, S. Z. Qiao, *Nat. Commun.* **2013**, *4*, 2798.

[35] L. L. Zhang, X. S. Zhao, *Chem. Soc. Rev.* **2009**, *38*, 2520.

[36] H. Jiang, J. Ma, C. Li, *Adv. Mater.* **2012**, *24*, 4197.

[37] X. Dong, Z. Guo, Y. Song, M. Hou, J. Wang, Y. Wang, Y. Xia, *Adv. Funct. Mater.* **2014**, *24*, 3405.

[38] X.-Q. Zhang, Q. Sun, W. Dong, D. Li, A.-H. Lu, J.-Q. Mu, W.-C. Li, *J. Mater. Chem. A* **2013**, *1*, 9449.

[39] D.-W. Wang, F. Li, M. Liu, G. Q. Lu, H.-M. Cheng, *J. Phys. Chem. C* **2008**, *112*, 9950.

[40] Y. Meng, D. Gu, F. Zhang, Y. Shi, L. Cheng, D. Feng, Z. Wu, Z. Chen, Y. Wan, A. Stein, D. Zhao, *Chem. Mater.* **2006**, *18*, 4447.

[41] Z. Li, D. Wu, Y. Liang, R. Fu, K. Matyjaszewski, *J. Am. Chem. Soc.* **2014**, *136*, 4805.

[42] L. Estevez, R. Dua, N. Bhandari, A. Ramanujapuram, P. Wang, E. P. Giannelis, *Energy Environ. Sci.* **2013**, *6*, 1785.

[43] X. Zhao, A. Wang, J. Yan, G. Sun, L. Sun, T. Zhang, *Chem. Mater.* **2010**, *22*, 5463.

[44] E. Kang, G. Jeon, J. K. Kim, *Chem. Commun.* **2013**, *49*, 6406.

[45] J. R. McDonough, J. W. Choi, Y. Yang, F. L. Mantia, Y. Zhang, Y. Cui, *Appl. Phys. Lett.* **2009**, *95*, 243109.

[46] C. Huang, Y. Wu, C. Hu, Y. Li, *J. Power Sources* **2007**, *172*, 460.

These are not the final page numbers! ↗↗

[47] G.-P. Hao, W.-C. Li, D. Qian, G.-H. Wang, W.-P. Zhang, T. Zhang, A.-Q. Wang, F. Schüth, H.-J. Bongard, A.-H. Lu, *J. Am. Chem. Soc.* **2011**, *133*, 11378.

[48] T. Y. Kim, H. W. Lee, M. Stoller, D. R. Dreyer, C. W. Bielawski, R. S. Ruoff, K. S. Suh, *ACS Nano* **2011**, *5*, 436.
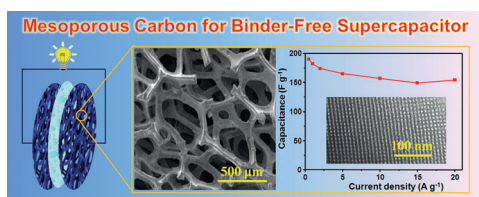
These are not the final page numbers! ↗↗

FULL PAPERS

X.-Q. Zhang, W. Dong, A.-H. Lu,
W.-C. Li*

■■ – ■■

**Rational Design of Mesoporous
Carbon Electrodes with High Mass
Loading for Binder-Free
Supercapacitors**

A binder-free mesoporous carbon electrode with high mass loading has been developed through an in situ solution synthesis strategy using nickel foam as conductive substrate and template. Benefited from a high surface area, hierarchical porosity, short diffusion path, and graphitic domains, such electrodes exhibit low contact resistance, high specific capacitance, and outstanding rate capability for use in supercapacitors.

© 2015 Wiley-VCH Verlag GmbH & Co. KGaA, Weinheim

These are not the final page numbers! ↗↗